Desalination and Water Treatment
www.deswater.com
doi: 10.5004/dwt.2022.28950

276 (2022) 309–318
November

The performance of an efficient solar domestic water heater based on an experimental study

S. Ettami[a,*], D. Saifaoui[a], A. Lilane[a], K. Gueddouch[b], Z. Boulahia[c]

[a]*Laboratory for Renewable Energy and Dynamic Systems, University Hassan II, Faculty of Science Ain Chock, El Jadida Road Km 9, BP 5366 Maarif, Casablanca, 20200 Morocco, emails: ettami-etu@etu.univh2c.ma/ettamisaid@gmail.com (S. Ettami), ddsaifaoui@gmail.com (D. Saifaoui), amine.lilane-etu@etu.univh2c.ma (A. Lilane)*
[b]*Laboratory of Materials and Volution of the Sciences and Techniques, Abdelmalek Essaadi University, Faculty of Sciences and Techniques, Tanger, Morocco, email: karima.gueddouch@gmail.com (K. Gueddouch)*
[c]*Laboratoire de Mécanique, BP 5366 Maarif, Casablanca, Morocco, email: boulahia.zoubair@gmail.com (Z. Boulahia)*

Received 18 March 2022; Accepted 23 September 2022

ABSTRACT

Urbanization, population and economic growth are nowadays among the major factors influencing the energy bill. This influence consequently leads to serious worldwide climate change. In the Moroccan context, this has pushed the country to a wise policy approach that allows it to increase the share of renewable energy, especially from solar and wind resources to improve energy efficiency. Approximately 93% of water is used for hygiene and cleaning, which consumes a lot of energy to heat it. In this context, a Flat Plate Collector (FPC) system is considered one of the most effective technologies since it is based on clean energy. Many people are in need for a FPC for domestic use. However, they can't afford buying because it is expensive. The aim of this work is essentially to study and realize a locally made prototype which adopts welding technique and uses "Latin" in order to reduce costs and make it affordable for many people due to its low price. This technique is cheaper than what is in the local market. To achieve the ultimate goal of this study, a modulating and interpretation of the results were done followed by a simulation using MATLAB software. Photothermal conversion was studied using a heat transfer fluid (water) whose temperature could reach up to 65°C through flat plate collector.

Keywords: Solar panel; FPC technologies; Solar collector modeling; Solar energy; Passive circulation system and FPC

1. Introduction

The Flat Plate Collector (FPC) is a simple system among the applications of solar thermal energy. It is considered most viable options to replace fossil fuel power plants [1]. The FPC is generally profitable when it is used to meet domestic and industrial needs (sanitary heating or pit heating). This actually justifies the huge investment made in these systems before and after the evacuated tube design [2,3]. Morocco is among the countries suitable for the implementation of solar energy projects in general, especially FPC projects. There are more than 750,000 m^2 of FPC installed in Morocco. Solar heating unit can be used for heating holy water or desalination in summer when solar potential is very high [4]. The thermal performance of FPC has gained more attention by researchers such as [5,6] in air conditioning [7,8], and power generation [9,10].

This study focuses on heating water using flat plate collector system. Laser welding technology is modern and effective, but it is a costly technique. In this article, an experimental study of a locally made prototype, which adopts welding techniques using Laitian was done and its results

* Corresponding author.

were interpreted and compared with the theoretical study. To achieve the main objective of this study, ten fins were made up and each fin includes coper tube and formed network absorbers. Additionally, a simulation using MATLAB software was done and several parameters such as total loss coefficient, the absorbed solar radiation, efficiency and other parameters were calculated [11].

2. Mathematical modeling of a flat plate collector

2.1. Incident radiation on Casablanca

Solar energy in most regions in Morocco is "usable". It is characterized by long duration of sunshine (Fig. 1) and solar radiation [12], which means that its use is economically viable [13]. The manufacture of a solar water heater begins first with a precise study of location (geographical location, climate, quantity of solar energy captured by the ground, etc.), then productivity can be determined per unit area from the global irradiation received by the collector. Then several parameters were calculated such as horizontal diffuse radiation, diffuse on tilted surface (Fig. 2b) and direct radiation for tilted surface (Fig. 2d).

Casablanca City is located on the Atlantic Coast in a very mild climate in the west of Morocco (Table 1). Its altitude at the level of the sea is 27 m, longitude is –7.7 and latitude ϕ = 33.6; the geographic data that we is needed to determine the solar field of Casablanca (like longitude and latitude) are reported in Table 1.

Daily performances of the flat panel collector depend on two parameters:

- Parameters thermal physics:
  An inlet temperature and outlet temperature of fluid.
  U_L: total loss.
  The properties of HTF (thermal conductivity).
- Geographical data:
  Solar radiation meteorological (data weather):
  Ambient temperature (Table 1).

If the physique parameters vary according to specific laws (heat transfer), parameters meteorological change substantially and randomly during the day (Table 2). Table 2 contains the majority of physical quantities that were calculated, including E_b; beam radiation on horizontal surface and E_g (global radiation on horizontal surface) etc. several hypothesis were suggested to make the calculation easy:

The system is stable; the fluid is unchangeable during the test; the stored energy in the form of heat inside which heats the systems supposed null.

After determining the parameters; h, δ, β, and ρ; the next step is the calculation of global solar radiation of tilted surface, which depends on β, γ, H and horizontal global solar radiation. While the calculation of reflected radiation on tilted surface is expressed in terms of Albedo, β, … Table 2 gives different values obtained for each of G_b, G_d, E_b, E_d, H, h, δ, β, ρ and G_g.

At a certain time of the year and at a specific time in the day, the position of the sun is therefore characterized by (a, h) for a fixed latitude.

As observed from Fig. 1, the changing of solar radiation (W/m²) in terms of time, the average values of the global radiation received by a 45° (Fig. 2), incident solar radiation on the solar collector, the ambient temperature and the beam of solar hourly radiation of Casablanca City [11,14] are illustrated. The curves mentioned in Fig. 2 clearly shows what was obtained in the Table 2.

Fig. 2 illustrates the changes in intensity of hourly global irradiation over time in Casablanca for a surface inclined at θ = 45° (Fig. 2a). Energy produced at the beginning and at the end of the day is lower than the energy produced when the sun is at its zenith (Fig. 2b and c). Fig. 2f presents the change of global irradiation over the time. We noticed through this curve that the value gradually increases to reach the maximum value (558 W/m²) and then gradually decreases.

The last line of the previous table (Table 1) shows values obtained for G_g which are also represented in the curve (Fig. 2b and c). Additionally, other parameters like… are also represented by (Fig. 2e and f).

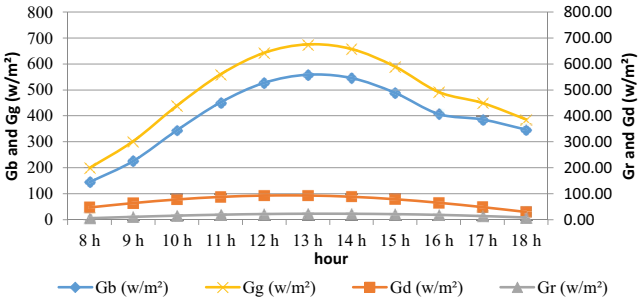

Fig. 1. Typical variation of solar radiation during a day: global (total) horizontal irradiation (G_g), beam radiation (G_b) on tilted surface, diffuse horizontal irradiation (G_d) and global irradiation incident (G_r) in Casablanca.

2.2. Absorbed solar flux

An inclined FPC receives three different components of solar radiation. The absorber effectively absorbs radiation (absorbency). After determining $(\tau\alpha)_b$ (direct absorbency), $(\tau\alpha)_d$ (diffuse absorbency) and $(\tau\alpha)_r$ (reflective absorbency), $G^a_{g,s}$ was calculated. It is represented mathematically as follows: [15,16] (1):

$$G^a_{g,s} = E_b \times R_b\left(\tau\alpha\right)_b + E_d\left(\tau\alpha\right)_d \times \frac{1+\cos\beta}{2} + \rho g\left(E_b + E_d\right)\left(\left(\tau\alpha\right)_r\right) \times \left(\frac{1+\cos\beta}{2}\right) \quad (1)$$

2.3. Thermal balance

The collector absorbs energy, which helps in heating flowing water in the tubes of the absorber [3]. Part of this energy dissipated by three transfer modes: convection, conduction and radiation (Q_p). In order to limit lost-heat, FPC is covered with an insulation; layers of glass wool (see the yellow color Fig. 4b). It is recommended to avoid thermal loss by using a 16 cm thickness of glass wool.

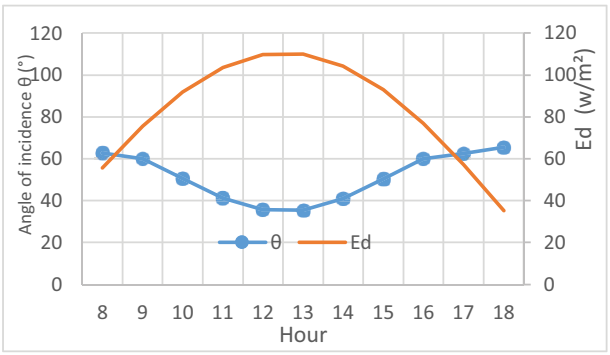

(a) Horizontal diffuse radiation depending of incidence angle.

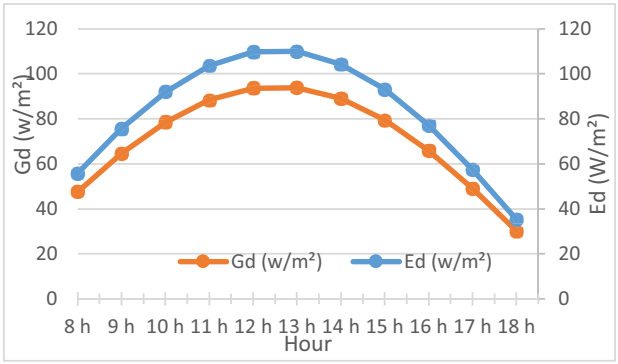

(b) Horizontal diffuse radiation and diffuse on tilted surface

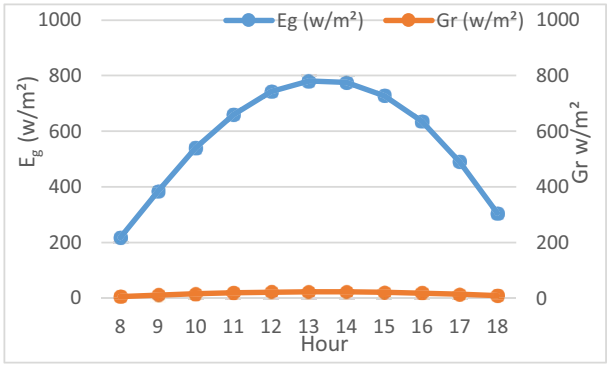

(c) Horizontal global radiation and radiation on tilted surface

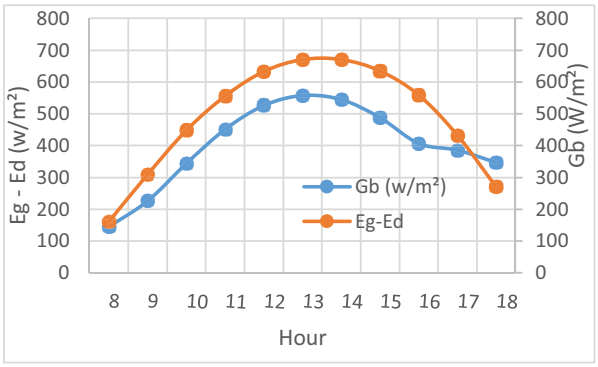

(d) Direct radiation for tilted surface

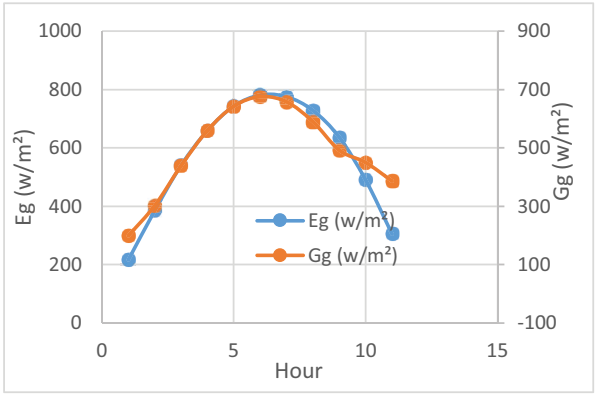

(e) Horizontal global irradiation and global of the tilted surface

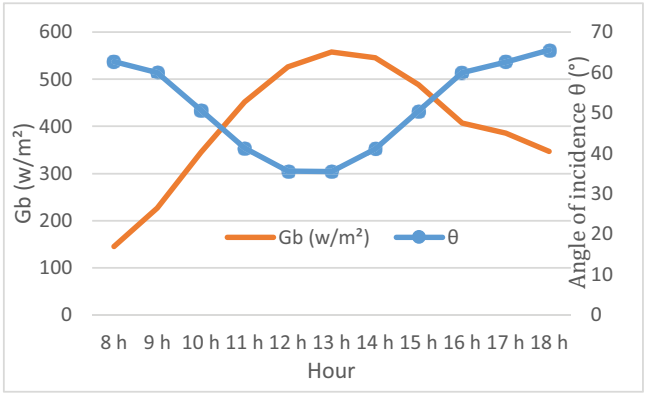

(f) Incidence angle and Gb of Casablanca city

Fig. 2. Horizontal radiation, diffuse, global on tilted surface and incidence angle. (a) Horizontal diffuse radiation depending of incidence angle. (b) Horizontal diffuse radiation and diffuse on tilted surface. (c) Horizontal global radiation and radiation on tilted surface. (d) Direct radiation for tilted surface. (e) Horizontal global radiation and global of the tilted surface. (f) Incidence angle and G_b of Casablanca City.

The following relation gives the thermal balance of a flat collector [17,18]:

$$A_c G^a_{g,s} = Q_u + Q_p + Q_s \quad (2)$$

where A_c: area of a flat collector; $G^a_{g,s}$: absorbed solar radiation/m² (W/m²); Q_u: useful energy gain/m²; Q_s: hot-stored-energy inside FPC system (In steady state or in case of low thermal inertia we will have Q_s = 0); Q_p: lost-energy [19].

$$Q_p = U_L \left(T_p - T_a\right) A_c \quad (3)$$

where T_p: average fluid temperature of absorber °C; T_a: ambient (air) temperature °C (Fig. 3a); U_L: total loss coefficient W/m²·K.

2.4. Useful heat gain

In steady state: $Q_s = 0$ (4)

Useful heat gain is different between absorbed power and thermal losses. It is represented by [20]:

$$Q_u = A_C \times \left(G_{g,s}^a - U_L\left(T_p - T_a\right)\right) \quad (5)$$

where A_c: is the surface of a flat collector (m²).

In order to calculate the heat loss of the panel, we use the coefficient below and the data from Table 3.

The thermal loss coefficient U_L [Eq. (6)] per unit area is given by [19,21]:

$$U_L = U_t + U_b + U_e \quad (6)$$

Table 1
Casablanca geographical data

Albedo ρ	0.2
Longitude *L*	–7.7
Azimuth γ	0
Slope of the FPC β	45
Latitude ϕ	33.6
Daylight saving time advanced or DST HAE	1
Place serving as a reference to legal time L_{ref}	0
Month	July
Day number of the year	183

The factor U_L includes heat losses by conduction, radiation and convection between various components of solar collector and the environment where [15]:

$$U_t = \left(\frac{N}{\frac{C}{T_p}\times\left[\frac{T_p - T_a}{N+f}\right]^e} + \frac{1}{h_w}\right)^{-1} + N - \frac{\sigma\times\left(T_a + T_p\right)\times\left(T_p^2 + T_a^2\right)}{\left(\varepsilon_p + 0.00591N\times h_w\right)^{-1} + \frac{2N + f - 1 + 0.133\varepsilon_p}{\varepsilon_v}} \quad (7)$$

where σ: Stefan–Boltzmann constant ($\sigma = 5.567\times10^{-8}$ W/m² K⁴); ε_v = 0.88 emissivity.

The convection coefficient is due to the movement of outside air [Eqs. (8) and (9)].

$$U_b = \frac{1}{R_3 + R_4} = \frac{1}{\frac{e}{k} + \frac{1}{h_w}} \quad (8)$$

Coefficient of heat transfer radiation is calculated using Eq. (11) as follows [22]:

$$h_{v-a} = h_w = f\left(V\right) \quad (9)$$

where *V*: is the wind speed (m/s).

Table 2
Global irradiation received by a 45° inclined area in Casablanca

Time	8 h	9 h	10 h	11 h	12 h	13 h	14 h	15 h	16 h	17 h	18 h
δ	23.44°	23.44°	23.44°	23.44°	23.44°	23.44°	23.44°	23.44°	23.44°	23.44°	23.44°
w_0	106.78°	106.78°	106.78°	106.78°	106.78°	106.78°	106.78°	106.78°	106.78°	106.78°	106.78°
ET (min)	–1.29	–1.29	–1.29	–1.29	–1.29	–1.29	–1.29	–1.29	–1.29	–1.29	–1.29
β	89.01°	89.01°	89.01°	89.01°	89.01°	89.01°	89.01°	89.01°	89.01°	89.01°	89.01°
TSV	7.49 h	8.49 h	9.49 h	10.49 h	11.49 h	12.49 h	13.49 h	14.49 h	15.49 h	16.49 h	17.49 h
w	–67.67°	–52.67°	–37.67°	–22.67°	–7.67°	7.33°	22.33°	37.33°	52.33°	67.33°	82.33°
TL_{Getup}	4.39 h	4.39 h	4.39 h	4.39 h	4.39 h	4.39 h	4.39 h	4.39 h	4.39 h	4.39 h	4.39 h
TL_{Sleep}	18.63 h	18.63 h	18.63 h	18.63 h	18.63 h	18.63 h	18.63 h	18.63 h	18.63 h	18.63 h	18.63 h
h	30.70°	43.12°	55.58°	67.69°	77.78°	77.94°	67.96°	55.87°	43.41°	30.99°	18.81°
γ	–80.76°	–88.20°	–82.76°	–68.70°	–35.36°	34.07°	68.25°	82.52°	88.38°	80.92°	73.85°
θ	62.70°	60.03°	50.68°	41.26°	35.60°	35.53°	41.08°	50.43°	59.97°	62.63°	65.53°
E_d (W/m²)	55.71	75.63	91.95	103.59	109.73	109.96	104.27	93.04	77.04	57.35	35.32
E_g (W/m²)	217.56	385.56	540.46	659.74	742.98	780.61	774.98	727.94	636.22	489.89	305.59
E_b (W/m²)	161.85	309.93	448.5	556.15	633.25	670.65	670.71	634.91	559.18	432.54	270.27
R_b	0.9	0.73	0.77	0.81	0.83	0.83	0.81	0.77	0.73	0.89	1.28
R_d	0.85	0.85	0.85	0.85	0.85	0.85	0.85	0.85	0.85	0.85	0.85
R_r	0.03	0.03	0.03	0.03	0.03	0.03	0.03	0.03	0.03	0.03	0.03
G_b (W/m²)	145.39	226.51	344.51	451.87	526.87	558.12	545.42	488.57	407.2	386.19	347.19
G_d (W/m²)	47.55	64.55	78.49	88.42	93.66	93.86	89	79.41	65.75	48.95	30.15
G_r (W/m²)	6.37	11.29	15.83	19.32	21.76	22.86	22.7	21.32	18.63	14.35	8.95
G_g (W/m²)	199.31	302.35	438.82	559.61	642.29	674.85	657.12	589.3	491.59	449.49	386.29

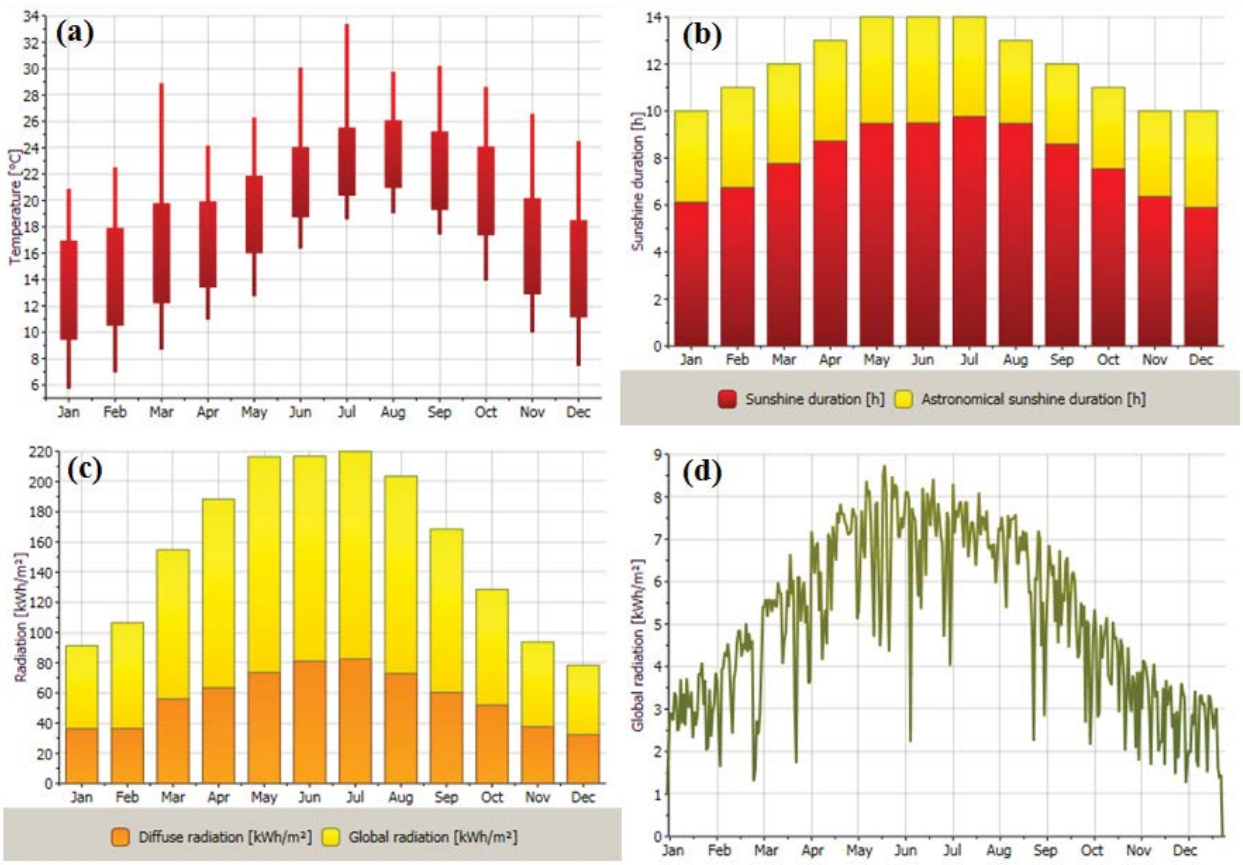

Fig. 3. (a) Ambient temperature variations of each month, (b) sunshine duration of each month, (c) diffuse and global radiation during a year, and (d) global radiation during a year.

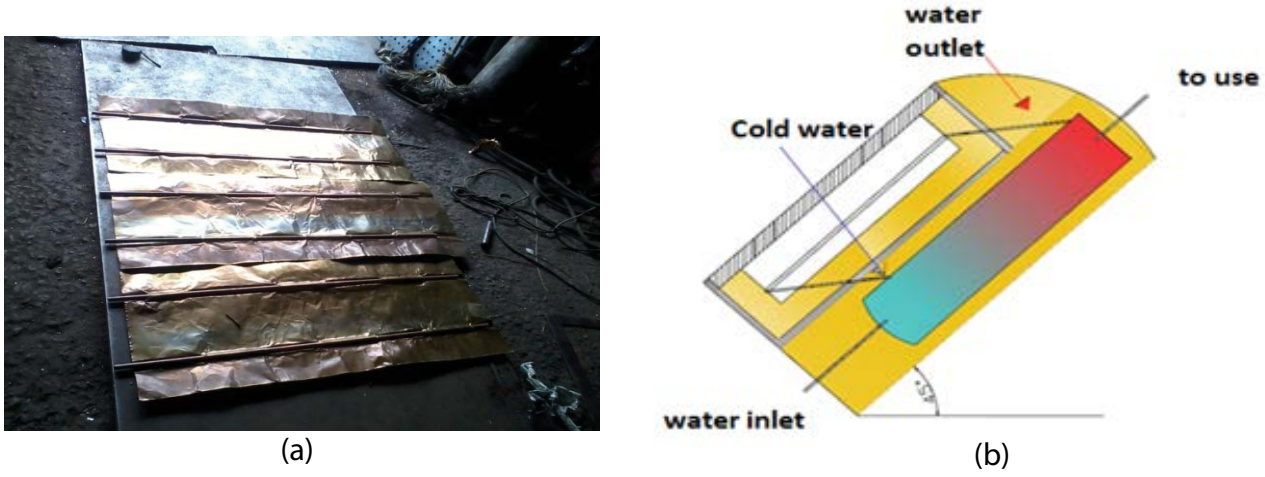

Fig. 4. (a) Absorber: a copper metal plate and (b) final CAD design of the set-up. Fig. 4b describes the prototype; it shows the inlet cold water and the inlet hot water coming from the absorber. It also indicates the position of the tank.

$$h_w = 5.7 + 3.8V \quad \text{Mc Adams (1954)} \tag{10}$$

The constants [15,23]:

$$f = \left(1 + 0.089\text{hw-}0.1166 \times \text{hw} \times \varepsilon p\right)\left(1 + 0.07866 \times N\right) \tag{11}$$

$$C = 520\left(1 - 51 \times 10^{-6} \times \beta^2\right) \tag{12}$$

Such as $70° \le \beta \le 70°$.
where β: inclination of a flat collector (45°).

Table 3
Prototype parameters

Setting	Meaning	Value
W	Distance between tubes (m)	0.2
D	Outer diameter of the tubes (m)	0.012
Di	Inner diameter of the tubes (m)	0.01
E	Thickness of the absorber (m)	0.0002
A	Absorber surface (m²)	1.2
Ka	Thermal conductivity of the absorber (copper) (W/m·°C)	380
ε_p	Emissivity of the absorber (–)	0.90
$\dot{m}$	Mass flow (kg/s)	0.03
C_p	Heat capacity of water (J/kg·°C)	4,180
T_{fi}	Fluid induct temperature (°C)	19
T_a	Ambient temperature (°C)	20.2
η_0	Optical efficiency	0.79
G_g	Absorbed solar radiation/m² (W/m²)	50,784
H	Height of a flat collector (m)	1.07
L_capt	Width of a flat collector (m).	1.25
e_capt	Thickness of a flat collector (m)	0.08
V	Wind speed (m/s)	2.6
β	Inclination of a flat collector (°)	45
ε_v	Emissivity of the glass (–)	0.88
N	Number of panels (–)	1
e	Insulation thickness (glass) (m)	0.05
K	Insulation conductivity (W/m²·°C)	0.044

$$e = 0.43\left(1 - \frac{100}{T_P + 273}\right) \tag{13}$$

With: T_p = 52°C.

2.5. Outlet temperature of fluid

By employing solar radiation as a thermal source, we can heat HTF (water) using CSP or FPC or any other heating system. Useful heat gain is the solar energy absorbed by the circulating water during the flow and through the absorber tube and is calculated using Eq. (16) as follows [24,25]:

$$\text{Qu} = m \times C_p \times \left(T_s - T_e\right) \tag{14}$$

From where outlet temperature of fluid can be expressed as Eq. (15):

$$T_s = \frac{\text{Qu}}{m \times C_p} + T_e \tag{15}$$

2.6. Efficiency of the system

Instantaneous optical efficiency is the ratio of the absorbed solar radiation to global radiation incident. It is calculated using Eq. (16) as follows [19,26]:

Table 4
Parameters results

Parameters	Meaning	Value
$G^a_{g,s}$ (absorbed)	Absorbed solar flux (W/m²)	507.84
T_p	Average fluid temperature of absorber (°C)	56
h_w	Convection coefficient (W/m²·K)	15.58
C	Constant (–)	466.29
f	Constant (W/m²·K)	0.713
U_t	Heat losses forward (W/m²·K)	6.04
U_b	Heat losses rearward (W/m²·K)	0.832
e	Thickness (m)	0.297
η_0	Instantaneous optical efficiency (–)	0.79

$$\eta_0 = \frac{G^a_{g,s}\left(\text{absorbed}\right)}{G_g\left(\text{incident}\right)} \tag{16}$$

This calculation determines the thermal characteristics of the solar collector, in which everything depends on incident solar radiation and received energy (Fig. 3d and c) by the absorber when this radiation exceeds the glass [27,28].

$$\eta = F_R\left[\frac{G^a_{g,s}}{G_{g,s}} - U_L \times \frac{T_{\text{fi}} - T_a}{A \times G_{g,s}}\right] \tag{17}$$

$$\eta = F_R\left[\eta_0 - U_L \times \frac{T_{\text{fi}} - T_a}{A \times G_{g,s}}\right] \tag{18}$$

3. System development

3.1. Description of the developed flat panel

After completing the theoretical study and determining the value of various basic parameters, these parameters were used during the manufacturing process of the prototype.

The FPC contains metal frame and a plate of glass. Under this glass, there is an absorber of welded copper that is painted in black (Fig. 4a). Ten copper tubes were used to make the absorber (forming what is called the tubular grid). The tubes were slipped in a line of omega form and welded using Laitan to make up the fins (Fig. 4a).

An insulation layer of glass wool provides insulation to the external environments. The tank and the cover in front of the panels are used to minimize losses and reduce the size and even shortening the passage by the fluid. The tank has a volume of 120 L and is oval, well fixed with metal sheets to build the panel. The water storage tank was constructed from galvanized sheet [29]. It is located behind the panel and attached to it to get good thermal insulation (Fig. 4). Fig. 4 presents all the elements that make up the FPC. Like all FPC, the prototype (Figs. 5 and 4) consists of an absorber located in an insulated formwork on the backside, glazing on the front side and tubes allowing

Fig. 5. Target prototype.

the passage of the heat transfer fluid. The three functions of the absorber are: absorb solar radiation, transform solar radiation into heat and transmit this heat to the heat transfer fluid. As shown in Figs. 4b and 5, water first entered the tubes through the flow rate and the temperature is increased because of the heat exchange with the absorber (inside the pipes) [30]. The heat transfer fluid rises up towards automatically (passive circulation system) [31]. Then the HTF was directed to the storage tank, because of the convection, without any circulating pump. This process is constantly repeated.

Fig. 4b describes the prototype; it shows the inlet cold water and the inlet hot water coming from the absorber. It also indicates the position of the tank.

The prototype was tested and installed in the rooftop, as shown in Fig. 5. The tests were carried out on the 5th of June from 8:00 am to 7:30 pm in Casablanca City in order to determine the effectiveness of the panel. The inlet temperature of water was 18°C, while the ambient temperature in the thermometer was 20. A digital thermometer was used to check the temperatures. On the testing day, the sky was clear; significant radiation, 5,972.11 W/m^2. Additionally, inclination of a flat collector is 45°. The data were collected and recorded at the end of each hour. Table 5 and 6 summarize the obtained results.

3.2. Panel parameters

The length and the width of the collector is 1.07 and 1.22 m, respectively. The spacing between the tubes is 0.2 m. Outer diameter of the tubes is 0.012 m and inner diameter is 0.01 m; a total of 10 tubes. Table 3 includes the main parameters.

3.3. Simulation of the system

MATLAB is an extremely flexible graphical based software which is used for dynamic simulation of renewable energy systems and building simulation. To simplify the calculations, a successive iterative method is used with a numerical simulation by MATLAB software because the value of $\Delta T \neq 0.01$°C (non-convergent).

One of the purpose of the study is to develop a calculation code to determine the temperature of output of the solar thermal collector according to the input temperature, methodological parameters, and characteristics of the panel under consideration.

Table 5
Results of iterative methods

U_L (W/m^2)	7.045
FR (–)	0.819
Q_u (W)	486.871
T_p (°C)	45.78
ΔT (°C)	0.01

Table 6
Variation of temperature absorber and global radiation by time

Hours	Measured global radiation, W/m^2	Absorber temperature, °C
8 h	189.31	21.0
9 h	300.35	23.5
10 h	430.82	25.0
11 h	551.61	27.0
12 h	652.29	30.0
13 h	674.85	34.1
14 h	670.12	36.8
15 h	589.30	38.4
16 h	491.59	40.0
17 h	444.49	44.0
18 h	379.29	47.6
19 h	314.90	53.8
19 h 30	300.00	56.0

MATLAB simulation is done according to the iterative diagram, and is developed on the basis of the above mathematical model and discrete method to characterize the performance of the prototype. The simulation program calculation flowchart is shown in Fig. 6 [22].

3.3.1. Simulation results by MATLAB program

The resolution of these equations allows the determination of the average temperature of: the absorber,

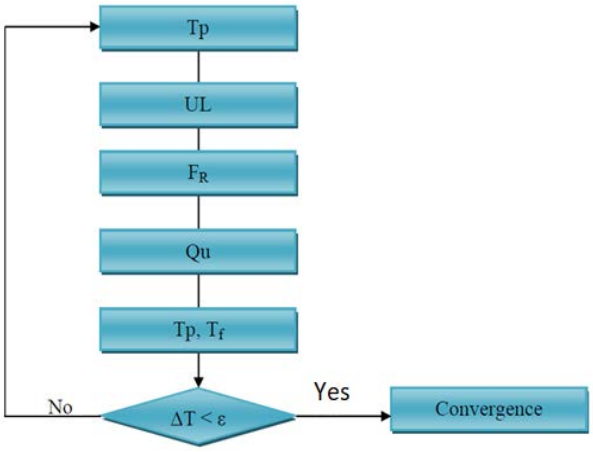

Fig. 6. Temperature calculation flowchart.

outlet and inlet temperature, tank temperature and all other parameters at the same time.

As illustrated in Fig. 7, variation of $G^{a}_{g,s}$ and useful energy gained by HTF according to time. It shows that there is an increasing change starting at 6 am until it reaches its maximum ($G^{a}_{g,s}$ = 700 W and Q_u = 486,87 W) and then starts the phase of regression. Note that Q_u is equal to 2/3 of $G^{a}_{g,s}$. On the other hand, Fig. 8 shows variation of a flat panel efficiency during the day; it is noticed that it increases in the morning to reach 0.6 and decreases rapidly at the end of the day due to the increase in temperature of the fluid that enters the a flat collector.

Fig. 9 where the *Y*-axis contains range variation of temperature in °C and the *X*-axis contains range of time. It shows the absorber and HTF temperature variation. Both values started to increase during the day until they reach the steady state [29].

3.4. Results and discussion

The experimental study was carried out in Casablanca City; during this experiment, a number of parameters were determined which are mentioned in Table 4.

After 10 iterance and at 12 o'clock in the morning, we obtained the following results in Table 5, which includes value of collector heat transfer factor, useful energy, absorber temperature and total loss coefficient.

As shown in Table 6, in both measured parameters (global radiation and absorbed temperature), there was a slight rise in water temperature at the beginning of the experiment and gradually rises in the afternoon. In addition, the temperature of the water inside the tank reaches 56°C by the end of the experiment.

Fig. 10 illustrates how the instantaneous efficiency changes; the change in thickness over time, both curves are an increasing exponential, and display the importance of absorber thickness in improving the efficiency of the fin and solar thermal collector. It also shows that beyond a thickness of 0.4 mm the efficiency of the FPC remains practically constant, which explains why the majority of manufacturers use thickness between 0.2 and 0.4 mm. That's why if a thickness of the absorber is greater than 0.6mm the efficiency of the daily approaches 1.

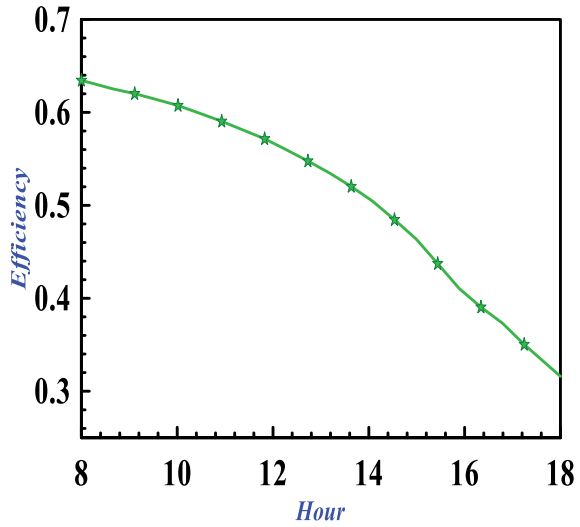

Fig. 7. Variation of useful energy and $G^{a}_{g,s}$ according to time increase in temperature of the fluid that enters the a flat collector.

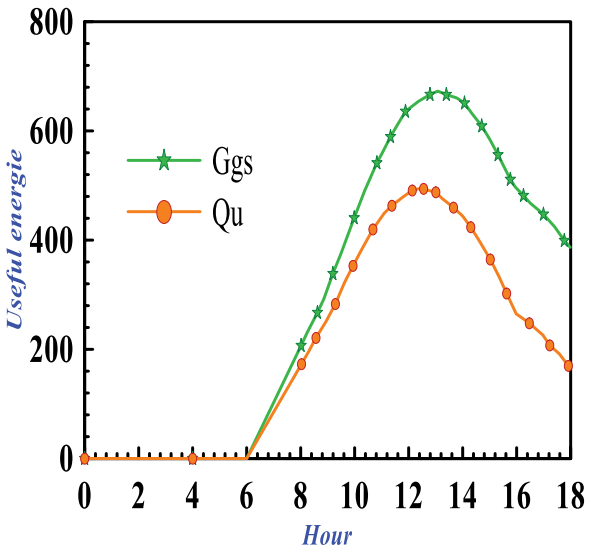

Fig. 8. Prototype efficiency variation.

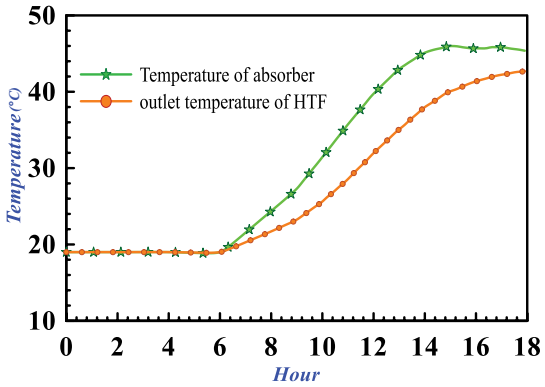

Fig. 9. Absorber and HTF temperature variation.

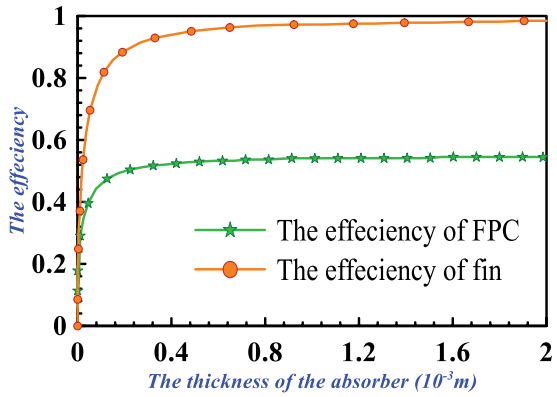

Fig. 10. Variation of efficiency as function of thickness.

4. Conclusion

In this work, a simulation of FPC using MATLAB software is illustrated. The experiment was mainly accomplished to produce a local prototype with lower cost and similar quality to what is available in the market. This system is cheap and only costs 2,500 dh (100 L tank size, 1.25 m^2) compared to traditional systems, which are highly costing and expensive (6,000 DH); and pollute environment (gas water heater). In this study, the optical efficiency was calculated and analysed. The obtained results of the experiment on the day of the test of the prototype, which was manufactured, are approximately of the same order of magnitude as the results expected from the theoretical study. Although the insolation is not very high, temperature of water in the storage tank reached 56°C at the end of the day while useful energy is Q_u = 486,871 W and instantaneous optical efficiency is η_0 = 0.79. As that, the simulation made it possible to observe the evolution of different methodological parameters and their influence on the efficiency of solar water heater. The results show that the presented prototype is effective in domestic water heating; however, it is not efficient in desalination, which will be the objective of our next articles.

Symbols

FR	—	Collector heat transfer factor
SF	—	Solar fraction (SF)
T_p	—	Average fluid temperature of absorber
U_L	—	Total loss coefficient
U_b	—	Heat losses rearward
U_t	—	Heat losses forward
Id	—	Effective incident beam radiation
N	—	Day number of the year
K_v	—	Thermal conductivity of the tube.
C_p	—	Specific heat capacity of fluid, J/K·kg
e_v	—	Tube thickness
q	—	Density of fluid, kg/m^3
L	—	Longitude
$G^a_{g,s}$	—	Absorbed solar radiation per square of aperture meter, W/m^2
h_w	—	Convection coefficient
E_b	—	Beam radiation on horizontal surface, W/m^2
$\dot{m}$	—	Mass flow
L_capt	—	Width of a flat collector
e_capt	—	Thickness of a flat collector
V	—	Wind speed
TL_{Getup}	—	Sunrise time
TL_{Sleep}	—	Sunset time
E_g	—	Global radiation on horizontal surface
E_d	—	Diffuse radiation on horizontal surface, W/m^2
R_r	—	Geometric factor
h	—	Height of the sun
w_0	—	Sunset hour angle
U_e	—	Lateral losses
HAF	—	Daylight saving time advanced or DST
ET	—	Equation of time (corrective term)
R_d	—	Ratio of diffuse radiation on tilted surface to that on horizontal surface
R_b	—	Ratio of beam radiation on tilted surface to that on horizontal surface
TSV	—	True solar time
g	—	Acceleration of gravity, m/s^2
Q_u	—	Useful energy gain per unit
Q_s	—	Stored energy inside which heats the system (Q_s = 0)
Q_p	—	Energy lost
G_b	—	Beam radiation on tilted surface, W/m^2
G_d	—	Diffuse radiation on tilted surface, W/m^2
G_r	—	Reflected radiation on tilted surface, W/m^2
G_g	—	Global radiation on tilted surface, W/m^2
T_a	—	Ambient air temperature, °C

Greek

Δ	—	Difference
Γ	—	Intercept factor
γ	—	Azimuth
τ	—	Transmittance
ϕ	—	Latitude
α	—	Absorbency
λ	—	Thermal conductivity, Wk/m^2
σ	—	The Stefan–Boltzmann constant 5.567 × 10^{-8} Wm^2/K^4
ε_v	—	Emissivity 0.88
β	—	Inclinaison of FPC
ε_p	—	Absorber plate emissivity, %
ΔT	—	Temperature difference (°C)
Γ	—	Intercept factor
δ	—	Declination angle
Θ	—	Incident angle of the beam irradiance
ρ	—	Albedo

References

[1] Y. Du, T.Y. Gao, G.T. Rochelle, A.S. Bhown, Zero- and negative-emissions fossil-fired power plants using CO_2 capture by conventional aqueous amines, Int. J. Greenhouse Gas Control, 111 (2021) 103473, doi: 10.1016/j.ijggc.2021.103473.

[2] F. Urban, S. Geall, Y. Wang, Solar PV and solar water heaters in China: different pathways to low carbon energy, Renewable Sustainable Energy Rev., 64 (2016) 531–542.

[3] A. Kumar, A. Raj, S. Kumar, J.P. Kesari, Development of solar powered air conditioner using flat plate collector, Mater. Today:. Proc., 47 (2021) 2883–2888.

[4] A. Chorak, P. Palenzuela, D.-C. Alarcón-Padilla, A. Ben Abdellah, Experimental characterization of a multi-effect distillation system coupled to a flat plate solar collector field: empirical correlations, Appl. Therm. Eng., 120 (2017) 298–313.
[5] R. Shukla, K. Sumathy, P. Erickson, J. Gong, Recent advances in the solar water heating systems: a review, Renewable Sustainable Energy Rev., 19 (2013) 173–190.
[6] S. Rehman, A.Z. Sahin, F.A. Al-Sulaiman, Economic assessment of industrial solar water heating system, FME Trans., 50 (2022) 16–23.
[7] B.M. Diaconu, S. Varga, A.C. Oliveira, Experimental assessment of heat storage properties and heat transfer characteristics of a phase change material slurry for air conditioning applications, Appl. Energy 87 (2010). 620–628.
[8] G. Li, Y. Hwang, R. Radermacher, Review of cold storage materials for air conditioning application, Int. J. Refrig., 35 (2012) 2053–2077.
[9] A. Gil, M. Medrano, I. Martorell, A. Lázaro, P. Dolado, B. Zalba, L.F. Cabeza, State of the art on high temperature thermal energy storage for power generation. Part 1—concepts, materials and modellization, Renewable Sustainable Energy Rev., 14 (2010) 31–55.
[10] L.C. Ding, N. Meyerheinrich, L. Tan, K. Rahaoui, R. Jain, A. Akbarzadeh, Thermoelectric power generation from waste heat of natural gas water heater, Energy Procedia, 110 (2017) 32–37.
[11] S. Ettami, D. Saifaoui, M. Oulhazzan, A. Gounni, Design and development of a parabolic solar concentrator, Mater. Today:. Proc., 30 (2020) 1021–1026.
[12] Y. El Mghouchi, T. Ajzoul, A. El Bouardi, Prediction of daily solar radiation intensity by day of the year in twenty-four cities of Morocco, Renewable Sustainable Energy Rev., 53 (2016) 823–831.
[13] G. He, Y. Zheng, Y. Wu, Z. Cui, K. Qian, Promotion of building-integrated solar water heaters in urbanized areas in China: experience, potential, and recommendations, Renewable Sustainable Energy Rev., 42 (2015) 643–656.
[14] S. ed-Dîn Fertahi, T. Bouhal, F. Gargab, A. Jamil, T. Kousksou, A. Benbassou, Design and thermal performance optimization of a forced collective solar hot water production system in Morocco for energy saving in residential buildings, Sol. Energy, 160 (2018) 260–274.
[15] Q. Ma, A. Ahmadi, C. Cabassud, Direct integration of a vacuum membrane distillation module within a solar collector for small-scale units adapted to seawater desalination in remote places: design, modeling & evaluation of a flat-plate equipment, J. Membr. Sci., 564 (2018) 617–633.
[16] S. Alqaed, Effect of using a solar hot air collector installed on the inclined roof of a building for cooling and heating system in the presence of polymeric PCM, Sustainable Energy Technol. Assess., 50 (2022) 101852, doi: 10.1016/j.seta.2021.101852.
[17] S.S. Nunayon, W.P. Akanmu, Potential application of a thermosyphon solar water heating system for hot water production in beauty salons: a thermo-economic analysis, Case Stud. Therm. Eng., 32 (2022) 101881, doi: 10.1016/j.csite.2022.101881.
[18] A. Shafieian, M. Khiadani, Integration of heat pipe solar water heating systems with different residential households: an energy, environmental, and economic evaluation, Case Stud. Therm. Eng., 21 (2020) 100662, doi: 10.1016/j.csite.2020.100662.
[19] S.A. Hakem, N. Kasbadji–Merzouk, M. Merzouk, Performances journalières d'un chauffe eau solaire, Rev. Energ. Renew. CICME, 8 (2008) 153–162.
[20] S.S. Nunayon, W.P. Akanmu, Potential application of a thermosyphon solar water heating system for hot water production in beauty salons: a thermo-economic analysis, Case Stud. Therm. Eng., 32 (2022) 101881, doi: 10.1016/j.csite.2022.101881.
[21] D. Zhang, H. Tao, M. Wang, Z. Sun, C. Jiang, Numerical simulation investigation on thermal performance of heat pipe flat-plate solar collector, Appl. Therm. Eng., 118 (2017) 113–126.
[22] M. Hu, C. Guo, B. Zhao, X. Ao, Suhendri, J. Cao, Q. Wang, S. Riffat, Y. Su, G. Pei, A parametric study on the performance characteristics of an evacuated flat-plate photovoltaic/thermal (PV/T) collector, Renewable Energy, 167 (2021) 884–898.
[23] J. Sarwar, M.R. Khan, M. Rehan, M. Asim, A.H. Kazim, Performance analysis of a flat plate collector to achieve a fixed outlet temperature under semi-arid climatic conditions, Sol. Energy, 207 (2020) 503–516.
[24] J. Shi, K. Lin, Z. Chen, H. Shi, Annual dynamic thermal performance of solar water heaters: a case study in China's Jiangsu Province, Energy Build., 173 (2018) 399–408.
[25] T. Baki, M. Tebbal, H. Berrebah, F. Bougara, Etude des performances d'un chauffe-eau solaire individuel installé à Oran, 1 Ère Conférences Sur Energ. Renouvelables Matér. Avancés ERMA'19, 2019.
[26] R. Daghigh, P. Zandi, An air and water heating system based on solar gas combined with nanofluids and phase change materials, J. Cleaner Prod., 311 (2021) 127751, doi: 10.1016/j.jclepro.2021.127751.
[27] S. Mohan, P. Dinesha, A.S. Iyengar, Modeling and analysis of a solar minichannel flat plate collector system and optimization of operating conditions using particle swarms, Therm. Sci. Eng. Prog., 22 (2021) 100855, doi: 10.1016/j.tsep.2021.100855.
[28] Z. Jiandong, T. Hanzhong, C. Susu, Numerical simulation for structural parameters of flat-plate solar collector, Sol. Energy, 117 (2015) 192–202.
[29] Y. Taheri, B.M. Ziapour, K. Alimardani, Study of an efficient compact solar water heater, Energy Convers. Manage., 70 (2013) 187–193.
[30] J.K. Kaldellis, K. El-Samani, P. Koronakis, Feasibility analysis of domestic solar water heating systems in Greece, Renewable Energy, 30 (2005) 659–682.
[31] B. Ghorbani, M. Mehrpooya, M. Sadeghzadeh, Developing a tri-generation system of power, heating, and freshwater (for an industrial town) by using solar flat plate collectors, multi-stage desalination unit, and Kalina power generation cycle, Energy Convers. Manage., 165 (2018) 113–126.